Antitumor Activity of Peptide Amphiphile Nanofiber-Encapsulated Camptothecin

Stephen Soukasene,[†,‡,⊥] Daniel J. Toft,[†,§,⊥] Tyson J. Moyer,[‡,⊥] Hsuming Lu,[‡] Hyung-Kun Lee,[‡] Stephany M. Standley,[‡] Vincent L. Cryns,[†,§,∥,*] and Samuel I. Stupp[†,‡,§,∥,*]

[†]Institute for BioNanotechnology in Medicine, Northwestern University, Chicago, Illinois 60611, United States, [‡]Department of Materials Science & Engineering, Northwestern University, Evanston, Illinois 60208, United States, and [§]Department of Medicine, Robert H. Lurie Comprehensive Cancer Center, Feinberg School of Medicine, Northwestern University, Chicago, Illinois 60611, United States. [⊥]These authors contributed equally to this work. [∥]These authors contributed equally to this work.

ABSTRACT

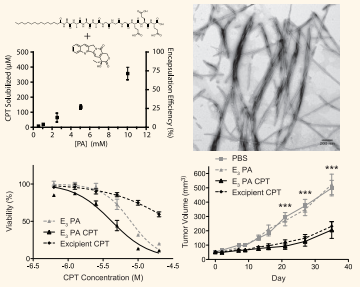

Self-assembling peptide amphiphile (PA) nanofibers were used to encapsulate camptothecin (CPT), a naturally occurring hydrophobic chemotherapy agent, using a solvent evaporation technique. Encapsulation by PA nanofibers was found to improve the aqueous solubility of the CPT molecule by more than 50-fold. PAs self-assembled into nanofibers in the presence of CPT as demonstrated by transmission electron microscopy. Small-angle X-ray scattering results suggest a slight increase in diameter of the nanofiber to accommodate the hydrophobic cargo. *In vitro* studies using human breast cancer cells show an enhancement in antitumor activity of the CPT when encapsulated by the PA nanofibers. In addition, using a mouse orthotopic model of human breast cancer, treatment with PA nanofiber-encapsulated CPT inhibited tumor growth. These results highlight the potential of this model PA system to be adapted for delivery of hydrophobic therapies to treat a variety of diseases including cancer.

KEYWORDS: peptide amphiphile · self-assembly · nanofiber · drug delivery · camptothecin · cancer therapy

In the field of therapeutic delivery, a variety of natural and synthetic nanomaterials[1−6] have been designed to incorporate bioactive components such as small molecules,[7−9] oligonucleotides,[9−11] and proteins[9,12−14] through noncovalent interactions. One strategy for noncovalently introducing therapeutic molecules into a system is to promote their physical encapsulation through hydrophobic collapse. Some pharmaceutical formulations, for example, use amphiphilic excipients, composed of hydrophobic and hydrophilic blocks, to form micelles that solubilize hydrophobic drugs in aqueous environments, thus improving their bioavailability.[6,15−20]

This concept of encapsulation by hydrophobic collapse has been explored in our laboratory using a unique class of peptide amphiphile (PA) molecules, which can self-assemble into high aspect ratio cylindrical nanofibers.[21,22] Compared to other modes of nanostructure fabrication, self-assembly has the advantage of facile generation of multiplexed nanostructures incorporating different molecular building blocks. PA molecules are composed of a sequence of amino acids linked to naturally occurring fatty acids. The self-assembly of the PA nanostructure is strongly dependent on the choice of peptide head group.[23] Assembly of PAs into filamentous nanostructures is based on a combination of hydrophobic collapse of the alkyl tails and hydrogen bonding in the β-sheet-forming region.[22] Aside from the inherent benefits of biocompatibility and biodegradability, the amino acid sequence of PAs can be modified to affect both the structural properties of the resulting nanofibers and their bioactivity. For example, PA nanostructures have been reported that display epitopes for specific receptors at concentrations that are easily controlled through co-assembly with non-bioactive molecules.[24,25] PAs have also been adapted for multiple biological applications including bone mineralization,[26] spinal cord regeneration,[27] angiogenesis,[28] cartilage regeneration,[29] and cancer therapy.[30]

Here, we examined the use of PA nanofibers for drug delivery with potential applications in cancer therapy. These nanostructures may be advantageous as cancer

* Address correspondence to v-cryns@northwestern.edu, s-stupp@northwestern.edu.

Received for review August 30, 2011 and accepted October 21, 2011.

Published online November 01, 2011
10.1021/nn203343z

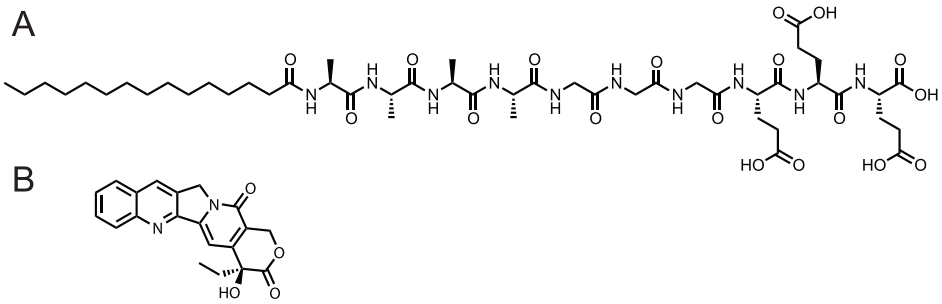

Figure 1. Chemical structures. (A) Chemical structure of the model "E_3 PA" peptide amphiphile used in these experiments with sequence palmitoyl-$A_4G_3E_3$. (B) Camptothecin in the active lactone form.

treatments through passive tumor targeting due to the enhanced permeability and retention (EPR) effect[31,32] and due to their shape, owing to enhanced bioavailability[33] and improved cellular uptake exhibited by high aspect ratio particles.[34,35] In the current work, a model PA (E_3 PA) was studied, which consisted of a hydrophobic palmitic tail linked to an $A_4G_3E_3$ sequence previously shown to self-assemble into the nanofiber morphology (Figure 1A).[36,37] The negative formal charge is included in the PA to increase solubility in water.

Camptothecin (CPT) was selected as the hydrophobic drug for encapsulation within the PA nanofiber (structure shown in Figure 1B). Discovered in 1966, CPT is a naturally occurring quinoline alkaloid originally extracted from the bark and stem of *Camptotheca acuminata*, a tree found in China and Tibet.[38] CPT induces cancer cell death by interfering with the actions of topoisomerase I, an essential enzyme in the DNA replication process.[39] Use of CPT in the clinic has been hindered by low aqueous solubility and its rapid conversion to a less active carboxylate form under physiological conditions. In this work, we demonstrated the ability of PA nanofibers to encapsulate and solubilize CPT, a challenging drug to formulate, and investigated the anticancer activity of the resulting nanostructures *in vitro* and *in vivo* using a murine model.

RESULTS AND DISCUSSION

PA Encapsulation of CPT. Encapsulation of CPT into PA nanofibers was achieved using a solvent evaporation technique that has been reported to yield near quantitative levels of encapsulation.[40,41] In this method, both the hydrophobic molecule and the amphiphile were mixed in a mutually dissolving solvent, which was removed by evaporation to produce a film, and then reconstituted in an aqueous medium. Aside from DMSO, which would not be a good candidate for solvent evaporation due to its high boiling point, HFIP was also found to dissolve both CPT and the E_3 PA. HFIP is well-known for dissolving and disaggregating proteins, peptides, and synthetic polyamides since it is a strong H-bond donor.[42−44] At concentrations of 10 mM and higher of the E_3 PA, dissolving in HFIP required gentle heating and sonication; however, an optically clear solution was eventually achieved. CPT was found to dissolve readily in HFIP at concentrations higher than 10 mM. We postulated that using HFIP as a mutual solvent promoted disaggregation of the individual components of the system, thereby improving mixing before water-induced hydrophobic collapse. Furthermore, the solvent evaporation proved to be a more rapid approach than dialysis techniques, which typically take several days to prepare encapsulated products.

Using the solvent evaporation method to encapsulate CPT in the PA nanostructures did indeed lead to high encapsulation efficiencies (Figure 2A). Encapsulation efficiencies were calculated by dividing the final concentration of encapsulated CPT by the original concentration of CPT added. When encapsulating a 0.5 mM initial concentration of CPT, an efficiency of 72% was observed for a 10 mM E_3 PA solution. This CPT encapsulation efficiency is higher than literature examples where loading efficiencies of 46−60% have been reported in block copolymer micelle systems using dialysis methods.[40,45] When using the PA to encapsulate CPT, aqueous solubility values as high as 360 μM CPT were observed, which is more than 50-fold higher than the solubility reported for CPT alone in water (7 μM).[46] Moreover, a near linear dependence on initial PA concentration was observed for the solubilization of CPT. A linear regression of the data estimates a molar ratio of 1:28 CPT to PA in the solubilized nanostructures. Fluorescence spectroscopy of PA-encapsulated CPT samples also suggests that the active lactone form of CPT is stabilized in the presence of PA even after 2 days under aqueous conditions. The spectrum of CPT in PA is blue-shifted relative to CPT alone in water (Figure 2B), which is consistent with the expected wavelength of the lactone (λ_{max} = 432 nm) compared to the carboxylate (λ_{max} = 446 nm) form.[47,48] Gradual release of the majority of CPT from PA nanofibers was observed over 1 week (Figure 2C). The time required for CPT release was similar to other nanoparticle constructs as previously reported.[49] This slow release limits the amount of free CPT present in circulation after systemic delivery, which could both reduce off-target systemic toxicity and allow for greater

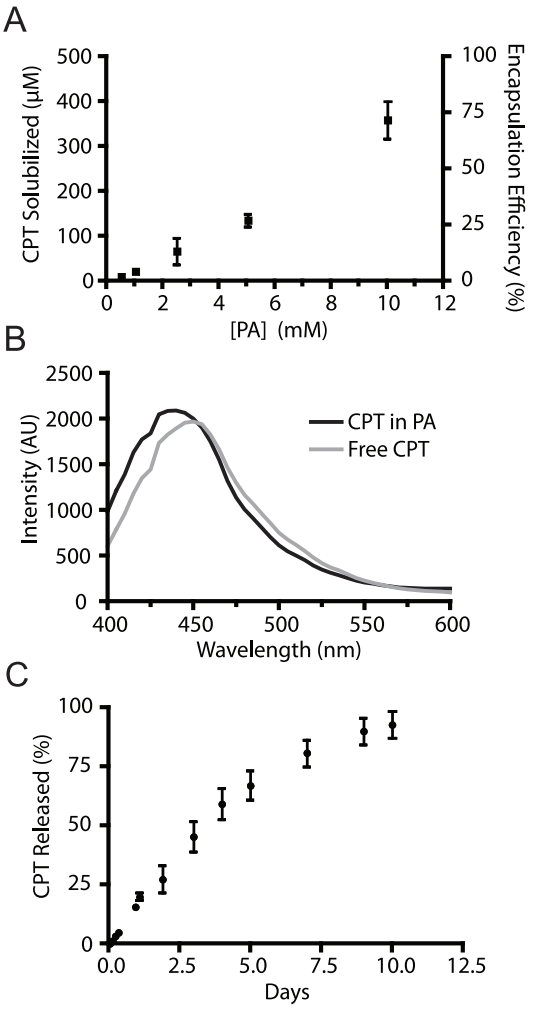

Figure 2. Peptide amphiphile nanofiber encapsulation of camptothecin. (A) Plot of E_3 PA-encapsulated CPT prepared by the solvent evaporation method *versus* the initial PA concentration used. The initial concentration of CPT was held constant at 0.5 mM. (B) Fluorescence spectra (360 nm excitation) of CPT encapsulated in E_3 PA nanofibers. (C) CPT-encapsulated PA (5 mM) was dialyzed in PBS over 12 days. The amount of CPT released was measured using fluorescence of the dialysate and normalized to the initial amount of CPT encapsulated by the PA.

accumulation of the PA-encapsulated CPT in tumor tissue.

After encapsulating CPT into the PA nanofibers, we used conventional TEM to qualitatively study their individual morphology (Figure 3). Average diameters of the fibers were measured to determine if incorporation of CPT induces swelling of the nanostructure. Average widths of 12.4 ± 2.6 and 11.9 ± 2.1 nm were observed for E_3 PA alone and E_3 PA with CPT, respectively. Therefore, fiber diameters did not appear to shift significantly in the presence of CPT, and the packing of the PA molecules into the cylinder shape was not hindered by the presence of the CPT molecule. A similar degree of fiber bundling was observed by TEM for both the PA alone and PA containing CPT.

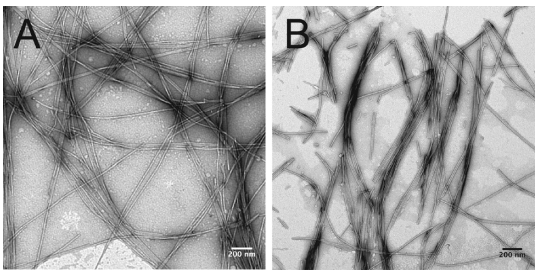

Figure 3. Transmission electron microscopy. (A) E_3 PA nanofibers and (B) E_3 PA-encapsulated CPT using the solvent evaporation method and reconstituted in PBS. There is no obvious change in fiber dimensions after CPT encapsulation. Bar = 200 nm.

We also studied nanofiber morphology by SAXS to characterize the shape and dimension of the nanostructures. The form factor of the 1-D scattering curve suggests the presence of long cylinders in solution, as evidenced by the −1 slope in the low-q range (Figure 4A).[50] Cross-sectional radii were determined using a modified Guinier analysis for cylindrical particles, which uses the slope of the plot of $\ln[ql(q)]$ *versus* q^2, where $I(q)$ is the scattering intensity.[51] The slope can be used to calculate the cross-sectional radius of gyration, $R_{G,c}$, by the following equation: $(R_{G,c})^2 = -2 \times$ slope. The value of $R_{G,c}$ is equal to $R/2^{1/2}$, where R is the actual radius of the cylinder. Slopes were determined in the linear portion of the low-q range ($qR_{G,c} < 1$). The decrease in slope of the E_3 PA with CPT compared to E_3 PA alone showed a slight increase in radius when CPT was added to the fiber structure (Figure 4B). From these slopes, the radius for E_3 PA was calculated to be 5.1 ± 0.19 nm and 5.5 ± 0.21 nm for E_3 PA with CPT. Both microscopy and scattering confirmed that the general high aspect ratio morphology of the E_3 PA nanofiber is undisturbed when loaded with drug. However, scattering experiments suggested that a small degree of swelling of the nanofibers might occur in order to accommodate a hydrophobic cargo.

***In Vitro* Activity of PA-Encapsulated CPT.** To investigate the antitumor activity of CPT encapsulated in E_3 PA nanofibers, we treated BT-474, MCF-7, and SKBR-3 human breast cancer cells for 24 h with varying concentrations of CPT alone or loaded into E_3 PA and measured cell viability using the CyQuant MTS assay (Figure 5). E_3 PA CPT was more cytotoxic than excipient CPT as reflected by lower IC_{50} values across all cell lines (Figure 5). However, the increased cytotoxicity *in vitro* was in part due to the unexpected toxicity of the encapsulating E_3 PA alone (Figure 5). The observed cytotoxicity was surprising as a PA with the peptide sequence $V_3A_3E_3$ (similar in charge to the $A_4G_3E_3$ used here) has been shown to act as a nanofiber gel scaffold supporting cell adhesion and proliferation.[52] We investigated the mechanism of E_3 PA-soluble nanofiber cytotoxicity in BT-474 cells. Treatment of BT-474 cells with 1.25 mM E_3 PA did not promote apoptosis as

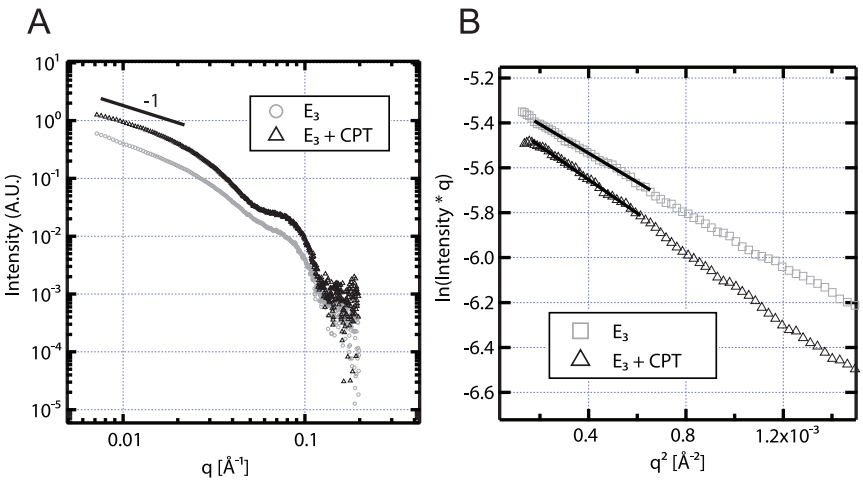

Figure 4. Small-angle X-ray scattering (SAXS) experiments. (A) SAXS patterns show a cylindrical form factor, as indicated by the −1 slope at low *q*. Both the E_3 PA and E_3 PA with encapsulated CPT show a similar scattering pattern, suggesting that the CPT does not disrupt the nanostructure. (B) Modified Guinier plot shows a change in slope in the Guinier regime ($qR_{G,c} < 1$) after encapsulation of CPT.

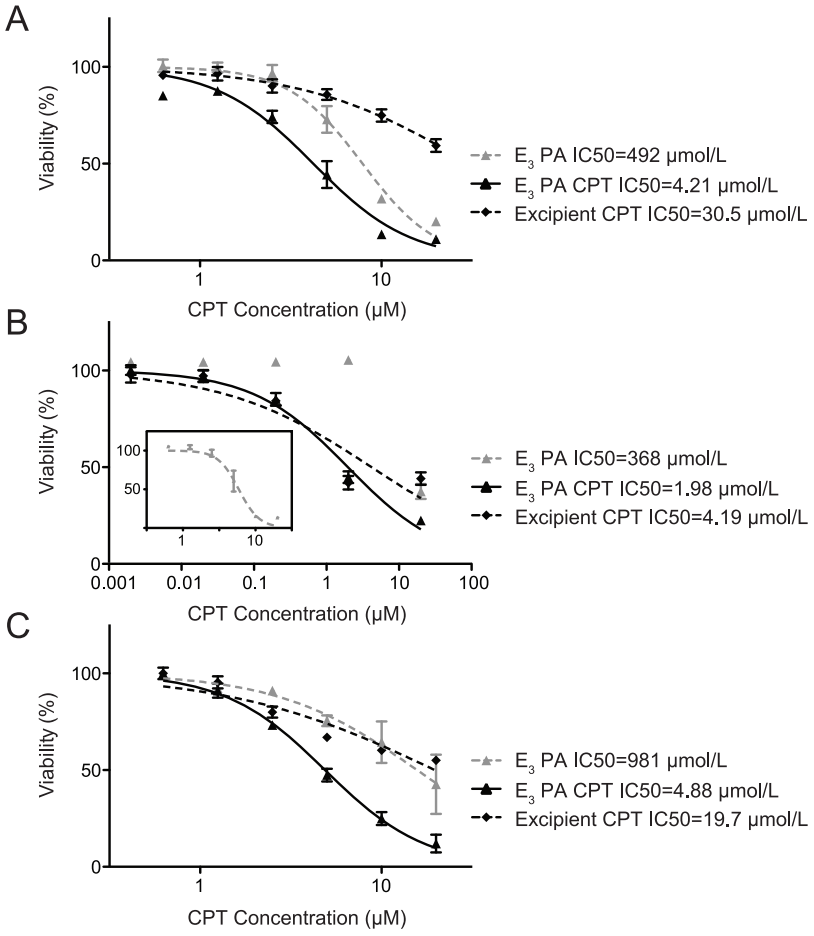

Figure 5. E_3 PA-encapsulated CPT is cytotoxic to breast cancer cells *in vitro*. (A) BT-474, (B) MCF-7, and (C) SKBR-3 cells treated with CPT alone and CPT encapsulated in E_3 PA nanofibers. Cell viability was measured by MTS assay (mean ± SEM, $n = 3$). To compare the toxicity of E_3 PA alone to the CPT-encapsulated E_3 PA, a CPT concentration based on a 1:62.5 molar ratio of CPT/E_3 PA was used.

measured by annexin V binding to externalized phosphatidylserine residues nor was cell toxicity rescued by pretreatment of cells with the pan-caspase inhibitor Z-VAD-FMK (data not shown). To determine if the

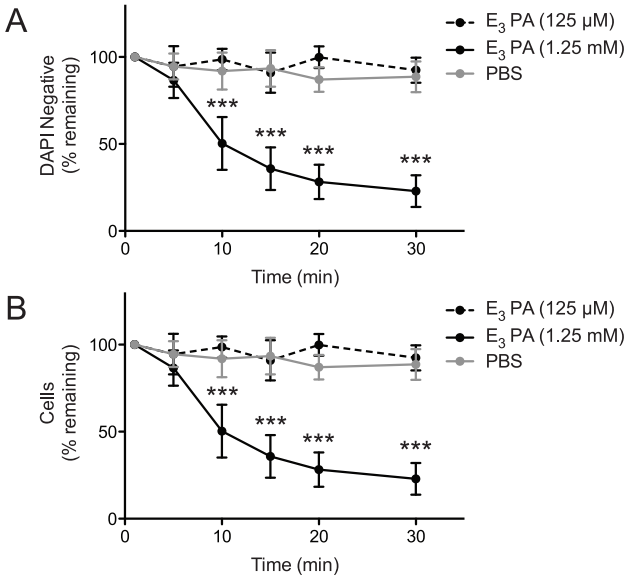

Figure 6. Soluble E_3 PA is membrane lytic at high concentrations. (A) BT-474 cells were treated with PBS, 20 or 200 μM E_3 PA in the presence of DAPI. The percent of cells in the DAPI-negative gate are shown over time. (B) BT-474 cellular concentration as measured as a ratio against time zero using fluorescent beads as an internal standard for each treatment group. Those cells that rapidly lose plasma membrane integrity are quickly lysed at the higher E_3 PA concentration.

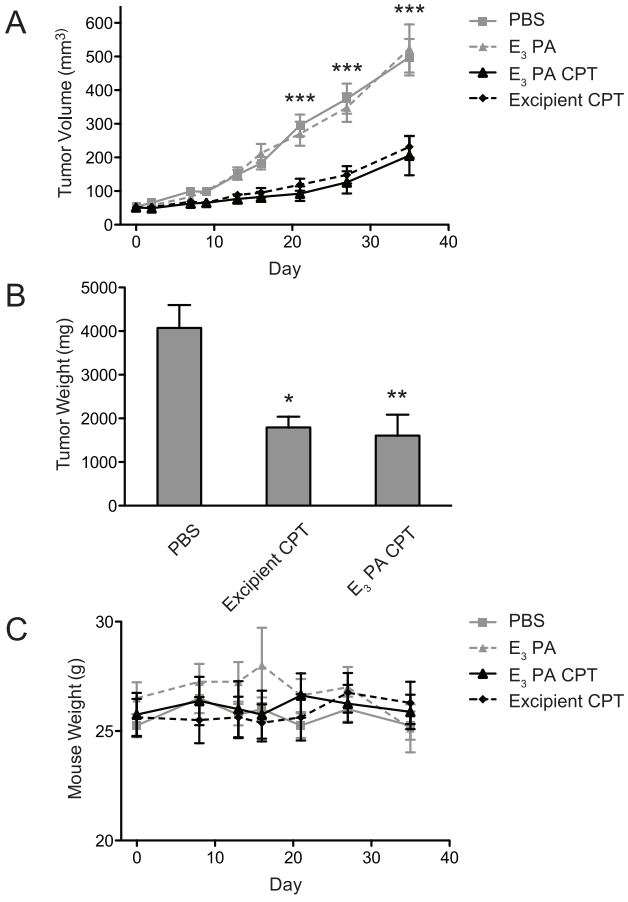

Figure 7. E_3 PA-encapsulated CPT inhibits breast cancer xenograft growth *in vivo*. (A) Plot of BT-474 breast tumors as a function of time. (B) Tumor weights at the end of the experiment show significant decreases for mice that have been treated with CPT. (C) Relative mouse weight over time during the treatments. No significant differences were observed between groups; * $p < 0.05$, ** $p < 0.01$, *** $p < 0.001$.

negatively charged E_3 PA was membrane lytic as we have seen previously with cationic PAs,[30] we performed flow cytometry-based time course experiments looking for plasma membrane permeability to the nuclear dye DAPI in response to E_3 PA treatment. As opposed to 125 μM E_3 PA treatment, cells exposed to 1.25 mM E_3 PA rapidly become DAPI-positive (Figure 6A), leading to rapid cellular lysis (Figure 6B), confirming the direct membrane lytic and cytotoxic action of these nanofibers at high concentrations.

Collectively, these *in vitro* studies suggest that the CPT has enhanced antitumor potential when encapsulated in the PA. We hypothesize that these results are a combination of the effects of stabilization of the active lactone form of CPT in the hydrophobic core of the PA, and at high concentrations, E_3 PA contributes to toxicity, as well. In future studies, the unexpected *in vitro* toxicity of the E_3 PA could be tempered with the addition of a polyethylene glycol chain to shield the negative charges, and hydrophobic cargo loading may be enhanced by using longer alkyl tails. PA nanofibers have been previously shown to become internalized by cells and metabolized through natural cellular processes,[34] which may improve drug uptake *in vivo*. To test the *in vivo* behavior of encapsulated CPT, we turned to a murine xenograft breast cancer model.

***In Vivo* Evaluation of Antitumor Activity.** The antitumor activity of PA-encapsulated CPT nanostructures was investigated *in vivo* using a BT-474 orthotopic xenograft model of breast cancer in athymic nude mice (Figure 7).[53,54] Four treatment groups were evaluated in the experiment, including (1) CPT encapsulated in PA; (2) a PA alone control; (3) a CPT control dissolved in a 7.5% excipient mixture in PBS v/v; and (4) a PBS vehicle control. The excipient mixture consisted of polyethylene glycol 400, propylene glycol, and polysorbate 80 (40:58:2), which has been used previously in the literature to dissolve CPT for *in vivo* studies.[55,56] The excipient components are commonly used in oral and injectable drug-solubilizing formulations.[57] Treatments were administered intravenously by tail vein injections, under the hypothesis that the EPR effect would enhance tumor uptake of the PA nanostructures. No statistically significant changes in weight of the mice were observed, suggesting that the treatments did not diminish their overall health (Figure 7C).

Measurement of the tumors over 3 weeks of injections showed a marked reduction in tumor growth in the mice injected with CPT relative to controls (Figure 7A). Any difference between the CPT in excipient formulation and the CPT encapsulated in PA, however, was difficult to discern quantitatively by tumor volumes or tumor weights (Figure 7A,B). While the CPT encapsulated in PA nanofibers exhibited a significant antitumor effect compared to the PBS vehicle and PA alone, the result was similar to the CPT in the excipient mixture. One explanation for the similarities in antitumor activity between the PA and excipient mixture is the presence of polysorbate 80, a nonionic surfactant, which could potentially sequester CPT into micelles.[58] Furthermore, it was also observed that nanoscale particles of CPT were observed to form in the excipient mixture, which, like the PA nanofibers, may be passively taken up in the tumors due to the EPR effect. Nonetheless, the PA nanofiber-encapsulated CPT demonstrated antitumor activity *in vivo* and shows promise for future therapies as further improvements are introduced in this platform of fully biodegradable nanostructures. One of the possibilities with these nanostructures is to integrate the therapeutic cargo with the use of PA molecules containing cytotoxic[30] or pro-apoptotic peptides as well as peptides that can target tumors.

CONCLUSIONS

We have demonstrated that peptide amphiphile nanofibers can be used to encapsulate the hydrophobic drug camptothecin in its biologically active lactone form. The method described yielded high encapsulation efficiencies and would be amenable to encapsulation of other molecules. We also demonstrated high efficacy for these systems *in vitro* and comparable efficacy *in vivo* compared to a positive control. These observations suggest that great therapeutic potential could be achieved with these systems compared to conventional excipients by using peptide amphiphiles that display targeting and cytotoxic or pro-apoptotic amino acid sequences. These bioactive and biodegradable constructs could increase cellular uptake and anticancer activity once the nanostructure extravasates into the tumor interstitium. These future directions are currently being explored in our laboratory.

MATERIALS AND METHODS

PA Synthesis. Synthesis of the E_3 PA was performed using standard Fmoc solid phase peptide synthesis protocols on a CS Bio CS136XT automated peptide synthesizer as previously described.[37] All fluorenylmethoxycarbonyl (Fmoc)-protected amino acids, Fmoc-Glu(OtBu)-Wang resin, and 2-(1*H*-benzotriazole-1-yl)-1,1,3,3-tetramethyluronium hexafluorophosphate (HBTU) were purchased from Novabiochem.

PA molecules were purified by reverse-phase HPLC using a Varian Prostar HPLC system and an X-bridge C-18 30 $\times$ 250 mm column. The mobile phase consisted of a water/acetonitrile (0.1% NH_4OH) or water/methanol (0.1% NH_4OH) gradient with a 25 mL/min flow rate. The desired HPLC fractions were combined, volatile organics were removed by rotary evaporation, and water was removed *via* lyophilization. Analytical HPLC (Varian, Phenomenex column) was performed to assess purity using a similar water/acetonitrile (0.1% NH_4OH) mobile phase

with a flow rate of 0.7 mL/min. Electrospray ionization mass spectrometry (ESI) measurements were performed, and observed masses corresponded with the desired product.

Preparation and Spectroscopic Characterization of CPT-Loaded PA Nanostructures. CPT was purchased from Sigma Aldrich and used without further chemical modification. Stock solutions of PA and CPT in HFIP (1,1,1,3,3,3-hexafluoro-2-propanol, 99.8+%, Sigma) were mixed together in a glass vessel and sonicated for 30 min in a 40 °C water bath. The vessel was then placed under vacuum with the cap loosened to allow evaporation of the solvent for a minimum of 2 h, which was sufficient to remove the HFIP. Aqueous media, such as purified water or PBS, was then added to the vessel, and the vessel was placed in a 40 °C water bath for 30 min in order to dissolve the dried material. Then the aqueous mixture was vortexed for 1 min, transferred to a centrifuge tube, and centrifuged at 1500*g* for 30 min to sediment undissolved CPT. The top 80% of the supernatant was then carefully removed and assayed for CPT concentration using a Molecular Devices microplate reader (ex = 360 nm, em = 450 nm). For storage, the remaining supernatant was then aliquoted, frozen in liquid nitrogen, and lyophilized. The dried material was stored at 4 °C or lower. Materials were reconstituted in aqueous media and mixed by vortex immediately prior to experiments. Assembly of nanofibers was observed by microscopy immediately after processing steps. Encapsulation efficiencies were calculated by dividing the concentration of encapsulated CPT by the initial concentration of CPT added and expressing the quotient as a percentage. CPT release studies were performed using a 1MWCO dialysis membrane (G-BioSciences). CPT-encapsulated PA (5 mM) was dissolved in PBS, added to a dialysis tube, and dialyzed in PBS over 12 days. The amount of CPT released was measured using fluorescence of the dialysate and normalized to the initial amount of CPT encapsulated by the PA. As a control formulation for biological assays, including *in vivo* studies, CPT was deposited from HFIP and dried as above, then dissolved in an excipient mixture of polyethylene glycol 400, propylene glycol, and polysorbate 80 (40:58:2), as used in the literature.[55,56]

Microscopy. Specimens for transmission electron microscopy (TEM) were prepared by drop-casting samples on carbon type B copper grids (Ted Pella) followed by staining with a 2% uranyl acetate aqueous solution. Images were taken using a JEOL 1230 transmission electron microscope operating at 100 keV equipped with a Hamamatsu ORCA camera.

Scattering Experiments. Small-angle X-ray scattering (SAXS) experiments were performed at the Advanced Photon Source, Argonne National Laboratory. The X-ray energy (15 keV) was selected using a double-crystal monochromator. The SAXS CCD camera was offset in order to achieve a wide range of scattering angles. Liquid samples were placed in 2.0 mm quartz capillary tubes. The typical incident X-ray flux on the sample was $\sim 1 \times 10^{12}$ photons/s with a 0.2×0.3 mm^2 collimator, estimated by a He ion channel. Samples were irradiated for 5 s. The 1D scattering profiles were obtained by radial integration of the 2D patterns, with scattering from the capillaries subtracted as background. Scattering profiles were then plotted on a relative scale as a function of the scattering vector $q = (4\pi/\lambda)\sin(\theta/2)$, where θ is the scattering angle.

Cell Culture and Reagents. The human breast cancer cell lines SKBR-3, MCF-7, and BT-474 were obtained from ATCC (Manasas, VA). Cell culture reagents were obtained from Invitrogen. SKBR-3 cells were grown in McCoy's 5A media, supplemented with 10% fetal bovine serum and 100 IU/mL penicillin-streptomycin. MCF-7 cells were maintained in MEM media with Earles' salts, 10% fetal bovine serum, 10 mM HEPES buffer, 2 mM L-glutamine, 0.1 mM non-essential amino acids, and 100 IU/mL penicillin-streptomycin. BT-474 cells were maintained in RPMI medium 1640 supplemented with 10% non-heat-inactivated FBS, 1 mM sodium pyruvate, 10 mM HEPES buffer, 10 μg/mL insulin, 2 mM L-glutamine, 2 g/L glucose, and 100 IU/mL penicillin-streptomycin. All cells were grown at 37 °C in 5% CO_2 atmosphere. 4′,6-Diamidino-2-phenylindole dihydrochloride (DAPI) was obtained from Sigma-Aldrich (St. Louis, MO).

Cell Viability Assays. Cell viability was measured using the CellTiter 96 Aqueous One Solution cell proliferation assay (Promega, Madison WI). The cell titer assay is a 3-(4,5-dimethylthiazol-2-yl)-5-(3-carboxymethoxyphenyl)-2-(4-sulfophenyl)-2*H*-tetrazolium (MTS)-based assay and was used as previously described according to the supplier's instructions. For each well to be assayed in a 96-well plate containing 100 μL of media per well, 20 μL of the CellTiter96 Aqueous One Solution was added. The plate was incubated for 1−3 h at 37 °C, and absorbance was read using a Molecular Devices microplate reader (490 nm).

Flow Cytometry Assays. Either E_3 PA or vehicle alone was added to BT-474 cells in suspension in the presence of 10 μg/mL DAPI. A time course of plasma membrane permeability and total cell concentration was determined by measuring fluorescence intensity at 25 °C using a DakoCyomation CyAn.

Mouse Orthotopic Xenograft Experiments. BT-474 human breast carcinoma cells (1×10^6) were implanted subcutaneously (s.c.) into the fourth mammary fat pads of 4−5 week old female athymic nude mice (Harlan Sprague−Dawley, Madison, WI) to establish orthotopic xenograft tumors. Mice were additionally supplemented with 17β-estradiol applied s.c. in a 60 day release biodegradable carrier binder (1.7 mg of estradiol per pellet) to promote xenograft tumor growth (Innovative Research of America). Four weeks after tumor implantation, mice were randomized into treatment groups (8 mice per group) and given 3 weeks of either PBS vehicle (Sigma-Aldrich), CPT 1.5 mg/kg/dose in an excipient formulation, CPT 1.5 mg/kg/dose encapsulated in 10 mM E_3 PA, and a 10 mM E_3 PA control by tail vein injection twice per week for six total injections. Tumors were measured after each injection with Vernier calipers, and tumor volume was calculated using the equation: tumor volume (mm^3) = (length $\times$ width^2) $\times$ π/6 as previously described.[54]

Acknowledgment. This work was supported by an NCI Center for Cancer Nanotechnology Excellence Grant 1U54CA119341 (S.I.S. and V.L.C.); the Breast Cancer Research Foundation (V.L.C.); Dixon Translational Research grant (V.L.C. and S.I.S.); Department of Defense Breast Cancer Research Program Grant W81XWH-10-1-0503 (D.J.T.); NIH Grants 5F32GM080021 (S.M.S.) and T32DK0-07169 (D.J.T.); and a Graduate Research Fellowship from the National Science Foundation (T.J.M.). Additional support was provided by the Northwestern University Flow Cytometry Facility and a Robert H. Lurie Comprehensive Cancer Center Support Grant (NCI CA060553). Transmission electron microscopy images were taken in the Biological Imaging Facility at Northwestern University. SAXS experiments were performed using the Advanced Photon Source DND-CAT beamline at Argonne National Laboratory. Use of the Advanced Photon Source at Argonne National Laboratory was supported by the U.S. Department of Energy under Contract No. DE-AC02-06CH11357. We thank Dr. Ronit Bitton, Dr. Honggang Cui, and Dr. Liam Palmer for helpful discussions.

REFERENCES AND NOTES

1. Allen, T. M.; Cullis, P. R. Drug Delivery Systems: Entering the Mainstream. *Science* **2004**, *303*, 1818–1822.
2. Langer, R. Biomaterials in Drug Delivery and Tissue Engineering: One Laboratory's Experience. *Acc. Chem. Res.* **2000**, *33*, 94–101.
3. LaVan, D. A.; Lynn, D. M.; Langer, R. Moving Smaller in Drug Discovery and Delivery. *Nat. Rev. Drug Discovery* **2002**, *1*, 77–84.
4. Lboutounne, H.; Faivre, V.; Falson, F.; Pirot, F. Characterization of Transport of Chlorhexidine-Loaded Nanocapsules through Hairless and Wistar Rat Skin. *Skin Pharmacol. Physiol.* **2004**, *17*, 176–182.
5. MacDonald, M. P.; Spalding, G. C.; Dholakia, K. Microfluidic Sorting in an Optical Lattice. *Nature* **2003**, *426*, 421–424.
6. Pillai, O.; Panchagnula, R. Polymers in Drug Delivery. *Curr. Opin. Chem. Biol.* **2001**, *5*, 447–451.
7. Zhang, J.; Ellsworth, K.; Ma, P. X. Hydrophobic Pharmaceuticals Mediated Self-Assembly of β-Cyclodextrin Containing Hydrophilic Copolymers: Novel Chemical Responsive Nano-Vehicles for Drug Delivery. *J. Controlled Release* **2010**, *145*, 116–123.
8. Zhang, W.; Rong, J.; Wang, Q.; He, X. The Encapsulation and Intracellular Delivery of Trehalose Using a Thermally

Responsive Nanocapsule. *Nanotechnology* **2009**, *20*, 275101.
9. Rolland, J. P.; Maynor, B. W.; Euliss, L. E.; Exner, A. E.; Denison, G. M.; DeSimone, J. M. Direct Fabrication and Harvesting of Monodisperse, Shape-Specific Nanobiomaterials. *J. Am. Chem. Soc.* **2005**, *127*, 10096–10100.
10. Vinogradov, S. V.; Batrakova, E. V.; Kabanov, A. V. Nanogels for Oligonucleotide Delivery to the Brain. *Bioconjugate Chem.* **2004**, *15*, 50–60.
11. Goh, S. L.; Murthy, N.; Xu, M.; Fréchet, J. M. Cross-Linked Microparticles as Carriers for the Delivery of Plasmid DNA for Vaccine Development. *Bioconjugate Chem.* **2004**, *15*, 467–474.
12. Liu, S. Q.; Yang, Y. Y.; Liu, X. M.; Tong, Y. W. Preparation and Characterization of Temperature-Sensitive Poly(*N*-isopropylacrylamide)-*b*-poly(D,L-lactide) Microspheres for Protein Delivery. *Biomacromolecules* **2003**, *4*, 1784–1793.
13. Pongjanyakul, T.; Medlicott, N. J.; Tucker, I. G. Melted Glyceryl Palmitostearate (GPS) Pellets for Protein Delivery. *Int. J. Pharm.* **2004**, *271*, 53–62.
14. Vila, A.; Sanchez, A.; Janes, K.; Behrens, I.; Kissel, T.; Vila Jato, J. L.; Alonso, M. J. Low Molecular Weight Chitosan Nanoparticles as New Carriers for Nasal Vaccine Delivery in Mice. *Eur. J. Pharm. Biopharm.* **2004**, *57*, 123–131.
15. Gupta, U.; Agashe, H. B.; Asthana, A.; Jain, N. K. Dendrimers: Novel Polymeric Nanoarchitectures for Solubility Enhancement. *Biomacromolecules* **2006**, *7*, 649–658.
16. Lee, C. C.; MacKay, J. A.; Frechet, J. M.; Szoka, F. C. Designing Dendrimers for Biological Applications. *Nat. Biotechnol.* **2005**, *23*, 1517–1526.
17. Liu, X. M.; Pramoda, K. P.; Yang, Y. Y.; Chow, S. Y.; He, C. Cholesteryl-Grafted Functional Amphiphilic Poly(*N*-isopropylacrylamide-*co*-*N*-hydroxylmethylacrylamide): Synthesis, Temperature-Sensitivity, Self-Assembly and Encapsulation of a Hydrophobic Agent. *Biomaterials* **2004**, *25*, 2619–2628.
18. Morgan, M. T.; Carnahan, M. A.; Immoos, C. E.; Ribeiro, A. A.; Finkelstein, S.; Lee, S. J.; Grinstaff, M. W. Dendritic Molecular Capsules for Hydrophobic Compounds. *J. Am. Chem. Soc.* **2003**, *125*, 15485–15489.
19. Rosler, A.; Vandermeulen, G. W.; Klok, H. A. Advanced Drug Delivery Devices *via* Self-Assembly of Amphiphilic Block Copolymers. *Adv. Drug Delivery Rev.* **2001**, *53*, 95–108.
20. Zupon, M. A.; Fang, S. M.; Christensen, J. M.; Petersen, R. V. *In Vivo* Release of Norethindrone Coupled to a Biodegradable Poly(α-amino acid) Drug Delivery System. *J. Pharm. Sci.* **1983**, *72*, 1323–1326.
21. Hartgerink, J. D.; Beniash, E.; Stupp, S. I. Peptide-Amphiphile Nanofibers: A Versatile Scaffold for the Preparation of Self-Assembling Materials. *Proc. Natl. Acad. Sci. U.S.A.* **2002** *99*, 5133–5138.
22. Hartgerink, J. D.; Beniash, E.; Stupp, S. I. Self-Assembly and Mineralization of Peptide-Amphiphile Nanofibers. *Science* **2001**, *294*, 1684–1688.
23. Trent, A.; Marullo, R.; Lin, B.; Black, M.; Tirrell, M. Structural Properties of Soluble Peptide Amphiphile Micelles. *Soft Matter* **2011**, *7*, 9572–9582.
24. Storrie, H.; Guler, M. O.; Abu-Amara, S. N.; Volberg, T.; Rao, M.; Geiger, B.; Stupp, S. I. Supramolecular Crafting of Cell Adhesion. *Biomaterials* **2007**, *28*, 4608–4618.
25. Guler, M. O.; Hsu, L.; Soukasene, S.; Harrington, D. A.; Hulvat, J. F.; Stupp, S. I. Presentation of RGDS Epitopes on Self-Assembled Nanofibers of Branched Peptide Amphiphiles. *Biomacromolecules* **2006**, *7*, 1855–1863.
26. Mata, A.; Geng, Y.; Henrikson, K. J.; Aparicio, C.; Stock, S. R.; Satcher, R. L.; Stupp, S. I. Bone Regeneration Mediated by Biomimetic Mineralization of a Nanofiber Matrix. *Biomaterials* **2010**, *31*, 6004–6012.
27. Tysseling-Mattiace, V. M.; Sahni, V.; Niece, K. L.; Birch, D.; Czeisler, C.; Fehlings, M. G.; Stupp, S. I.; Kessler, J. A. Self-Assembling Nanofibers Inhibit Glial Scar Formation and Promote Axon Elongation After Spinal Cord Injury. *J. Neurosci.* **2008**, *28*, 3814–3823.
28. Rajangam, K.; Behanna, H. A.; Hui, M. J.; Han, X.; Hulvat, J. F.; Lomasney, J. W.; Stupp, S. I. Heparin Binding Nanostructures To Promote Growth of Blood Vessels. *Nano Lett.* **2006**, *6*, 2086–2090.
29. Shah, R. N.; Shah, N. A.; Del Rosario Lim, M. M.; Hsieh, C.; Nuber, G.; Stupp, S. I. Supramolecular Design of Self-Assembling Nanofibers for Cartilage Regeneration. *Proc. Natl. Acad. Sci. U.S.A.* **2010**, *107*, 3293–3298.
30. Standley, S. M.; Toft, D. J.; Cheng, H.; Soukasene, S.; Chen, J.; Raja, S. M.; Band, V.; Band, H.; Cryns, V. L.; Stupp, S. I. Induction of Cancer Cell Death by Self-Assembling Nanostructures Incorporating a Cytotoxic Peptide. *Cancer Res.* **2010**, *70*, 3020–3026.
31. Matsumura, Y.; Maeda, H. A New Concept for Macromolecular Therapeutics in Cancer Chemotherapy: Mechanism of Tumoritropic Accumulation of Proteins and the Antitumor Agent Smancs. *Cancer Res.* **1986**, *46*, 6387–6392.
32. Duncan, R. The Dawning Era of Polymer Therapeutics. *Nat. Rev. Drug Discovery* **2003**, *2*, 347–360.
33. Geng, Y.; Dalhaimer, P.; Cai, S.; Tsai, R.; Tewari, M.; Minko, T.; Discher, D. E. Shape Effects of Filaments *versus* Spherical Particles in Flow and Drug Delivery. *Nat. Nanotechnol.* **2007**, *2*, 249–255.
34. Beniash, E.; Hartgerink, J. D.; Storrie, H.; Stendahl, J. C.; Stupp, S. I. Self-Assembling Peptide Amphiphile Nanofiber Matrices for Cell Entrapment. *Acta Biomater.* **2005**, *1*, 387–397.
35. Gratton, S. E.; Ropp, P. A.; Pohlhaus, P. D.; Luft, J. C.; Madden, V. J.; Napier, M. E.; DeSimone, J. M. The Effect of Particle Design on Cellular Internalization Pathways. *Proc. Natl. Acad. Sci. U.S.A.* **2008**, *105*, 11613–11618.
36. Lee, H. K.; Soukasene, S.; Jiang, H.; Zhang, S.; Feng, W.; Stupp, S. I. Light-Induced Self-Assembly of Nanofibers Inside Liposomes. *Soft Matter* **2008**, *4*, 962–964.
37. Niece, K. L.; Czeisler, C.; Sahni, V.; Tysseling-Mattiace, V.; Pashuck, E. T.; Kessler, J. A.; Stupp, S. I. Modification of Gelation Kinetics in Bioactive Peptide Amphiphiles. *Biomaterials* **2008**, *29*, 4501–4509.
38. Wall, M. E.; Wani, M. C.; Cook, C. E.; Palmer, K. H.; Mephail, A. T.; Sim, G. A. Plant Antitumor Agents. 1. The Isolation and Structure of Camptothecin, a Novel Alkaloidal Leukemia and Tumor Inhibitor from *Camptotheca acuminata*. *J. Am. Chem. Soc.* **1966**, *88*, 3888–3890.
39. Hsiang, Y. H.; Hertzberg, R.; Hecht, S.; Liu, L. F. Camptothecin Induces Protein-Linked DNA Breaks *via* Mammalian DNA Topoisomerase I. *J. Biol. Chem.* **1985**, *260*, 14873–14878.
40. Yokoyama, M.; Opanasopit, P.; Okano, T.; Kawano, K.; Maitani, Y. Polymer Design and Incorporation Methods for Polymeric Micelle Carrier System Containing Water-Insoluble Anti-Cancer Agent Camptothecin. *J. Drug Target* **2004**, *12*, 373–384.
41. Lavasanifar, A.; Samuel, J.; Kwon, G. S. Micelles Self-Assembled from Poly(ethylene oxide)-*block*-Poly(*N*-hexyl stearate L-aspartamide) by a Solvent Evaporation Method: Effect on the Solubilization and Haemolytic Activity of Amphotericin B. *J. Controlled Release* **2001**, *77*, 155–160.
42. Crisma, M.; Saviano, M.; Moretto, A.; Broxterman, Q. B.; Kaptein, B.; Toniolo, C. Peptide α/3(10)-Helix Dimorphism in the Crystal State. *J. Am. Chem. Soc.* **2007**, *129*, 15471–15473.
43. Ha, S. W.; Asakura, T.; Kishore, R. Distinctive Influence of Two Hexafluoro Solvents on the Structural Stabilization of Bombyx Mori Silk Fibroin Protein and Its Derived Peptides: ^{13}C NMR and CD Studies. *Biomacromolecules* **2006**, *7*, 18–23.
44. Sirangelo, I.; Dal Piaz, F.; Malmo, C.; Casillo, M.; Birolo, L.; Pucci, P.; Marino, G.; Irace, G. Hexafluoroisopropanol and Acid Destabilized Forms of Apomyoglobin Exhibit Structural Differences. *Biochemistry* **2003**, *42*, 312–319.
45. Opanasopit, P.; Yokoyama, M.; Watanabe, M.; Kawano, K.; Maitani, Y.; Okano, T. Block Copolymer Design for Camptothecin Incorporation into Polymeric Micelles for Passive Tumor Targeting. *Pharm. Res.* **2004**, *21*, 2001–2008.
46. Greenwald, R. B.; Choe, Y. H.; McGuire, J.; Conover, C. D. Effective Drug Delivery by PEGylated Drug Conjugates. *Adv. Drug Delivery Rev.* **2003**, *55*, 217–250.

47. Dey, J.; Warner, I. M. Spectroscopic and Photophysical Studies of the Anticancer Drug: Camptothecin. *J. Lumin.* **1997**, *71*, 105–114.
48. Chourpa, I.; Millot, J.-M.; Sockalingum, G. D.; Riou, J.-F.; Manfait, M. Kinetics of Lactone Hydrolysis in Antitumor Drugs of Camptothecin Series As Studied by Fluorescence Spectroscopy. *Biochim. Biophys. Acta* **1998**, *1379*, 353–366.
49. Liu, J.; Jiang, Z.; Zhang, S.; Saltzman, W. M. Poly(ω-pentadecalactone-*co*-butylene-*co*-succinate) Nanoparticles as Biodegradable Carriers for Camptothecin Delivery. *Biomaterials* **2009**, *30*, 5707–5719.
50. Glatter, O.; Kratky, O. *Small Angle X-ray Scattering*; Academic Press: New York, 1982.
51. Burkoth, T. S.; Benzinger, T. L. S.; Urban, V.; Lynn, D. G.; Meredith, S. C.; Thiyagarajan, P. Communications to the Editor—Self-Assembly of Ab(10−35)-PEG Block Copolymer Fibrils. *J. Am. Chem. Soc.* **1999**, *121*, 2.
52. Webber, M. J.; Tongers, J.; Renault, M.-A.; Roncalli, J. G.; Losordo, D. W.; Stupp, S. I. Development of Bioactive Peptide Amphiphiles for Therapeutic Cell Delivery. *Acta Biomater.* **2010**, *6*, 3–11.
53. Kamradt, M. C.; Lu, M.; Werner, M. E.; Kwan, T.; Chen, F.; Strohecker, A.; Oshita, S.; Wilkinson, J. C.; Yu, C.; Oliver, P. G.; Duckett, C. S.; Buchsbaum, D. J.; LoBuglio, A. F.; Jordan, V. C.; Cryns, V. L. The Small Heat Shock Protein α B-Crystallin Is a Novel Inhibitor of TRAIL-Induced Apoptosis That Suppresses the Activation of Caspase-3. *J. Biol. Chem.* **2005**, *280*, 11059–11066.
54. Lu, M.; Kwan, T.; Yu, C.; Chen, F.; Freedman, B.; Schafer, J. M.; Lee, E. J.; Jameson, J. L.; Jordan, V. C.; Cryns, V. L. Peroxisome Proliferator-Activated Receptor γ Agonists Promote TRAIL-Induced Apoptosis by Reducing Survivin Levels *via* Cyclin D3 Repression and Cell Cycle Arrest. *J. Biol. Chem.* **2005**, *280*, 6742–6751.
55. Watanabe, M.; Kawano, K.; Toma, K.; Hattori, Y.; Maitani, Y. *In Vivo* Antitumor Activity of Camptothecin Incorporated in Liposomes Formulated with an Artificial Lipid and Human Serum Albumin. *J. Controlled Release* **2008**, *127*, 231–238.
56. Yang, S. C.; Lu, L. F.; Cai, Y.; Zhu, J. B.; Liang, B. W.; Yang, C. Z. Body Distribution in Mice of Intravenously Injected Camptothecin Solid Lipid Nanoparticles and Targeting Effect on Brain. *J. Controlled Release* **1999**, *59*, 299–307.
57. Katdare, A.; Chaubal, M. V. *Excipient Development for Pharmaceutical, Biotechnology, and Drug Delivery Systems*; Informa Healthcare: London, **2006**.
58. Aizawa, H. Morphology of Polysorbate 80 (Tween 80) Micelles in Aqueous 1,4-Dioxane Solutions. *J. Appl. Crystallogr.* **2009**, *42*, 592–596.